Research Article

Yaoqun Xu, Juan Wang*, Peng Zhang, Jinjun Guo, and Shaowei Hu

Effect of micron-scale pores increased by nano-SiO₂ sol modification on the strength of cement mortar

https://doi.org/10.1515/ntrev-2022-0139 received December 31, 2021; accepted June 7, 2022

Abstract: A study was conducted through quantitative calculations on the correlation between the micron-scale pores and the strength of nano-SiO2 (NS) sol reinforced cement mortar. The strength, pore structure, and microstructure of NS sol modified mortar were investigated, and the mortars were made equivalent to a two-phase material comprised of pores and mortar matrix; the model was applied to conduct a quantitative analysis of the correlation between pores and the strength. According to the research results, the modification made to the mortar using the NS sol led to significantly increased early strength and the level of porosity was also increased. Furthermore, the addition of NS caused a change to the C-S-H gel morphology of cement hydration products. As revealed by the results of quantitative analysis, the addition of 1.5 and 3% NS improved the mortar matrix strength by 29.3 and 56.6%, respectively. Moreover, the ratio between the mortar strength (f_c) and matrix strength index (K) exhibited a nonlinear correlation with the porosity negatively. It was thus inferred that the increase in mortar porosity inhibited the improvement of mortar strength under the influence of NS sol.

Keywords: nano-SiO₂ sol, micron-scale pores, mechanical properties, cement mortar

1 Introduction

Admixtures and fibers can be added to cementitious materials to achieve high performances and long lifetimes [1–3]. The use of nanomaterials has been proven to be one of the most effective methods for reinforcing cementitious materials [4–6]. Incorporating a small amount of nanoparticles in concrete can modify the nano-structure of cementitious materials, and thus procure high durability [7].

Nano-SiO₂ (NS) is the most extensively used nanomaterial for cementitious materials [8,9]. Many researchers have focused on the effects of NS modification on the various characteristics of cementitious materials. Xu et al. [10] found that NS enhanced the elastic modulus ratio of the interfacial transition zone to cement paste increases from approximately 50 to 80%. And the strength of the cement paste was enhanced by 20–28% at an age of 28 days [11], and the strength of mortar with 12% NS particles was enhanced by 77% at an age of 7 days [12]. In relation to durability, NS can enhance the sulfate resistance of concrete [13]. In the study of Zhang and Li [14], the chloride permeability coefficient of NS-modified concrete was significantly reduced. In a test of the scanning electron microscope (SEM), the microstructure compactness of cement composites is improved by NS [15,16]. In addition, the frost resistance of the NS-modified concrete was improved [17,18], and the concrete water absorption rate could be decreased by the NS modification [19]. Zhang et al. [20] found that NS could greatly improve the impact resistance of steel fiber concrete. In the study of Li et al. [21], the service lives of coated concrete against chloride attack can be lengthened by 7.1 times 0.5% NS are added into the coating.

Although NS can improve the overall performance of cementitious materials, the excellent performance provided by NS modification is not fully utilized when the NS particles form aggregates in the cement matrix [22,23]. New industrial sols have been stable for long periods,

^{*} Corresponding author: Juan Wang, Yellow River Laboratory, Zhengzhou University, Zhengzhou, Henan 450001, China; State Key Laboratory of Hydroscience and Engineering, Tsinghua University, Beijing 100000, China, e-mail: wangjuan@zzu.edu.cn
Yaoqun Xu, Peng Zhang, Jinjun Guo, Shaowei Hu: School of Water Conservancy Engineering, Zhengzhou University, Zhengzhou, Henan 450001, China; Yellow River Laboratory, Zhengzhou University, Zhengzhou, Henan 450001, China

which has significantly promoted the extensive application of nanomaterials [24,25]. Attempts have been made to use an NS sol to solve the issue of silica nanoparticle dispersion in cement [26,27]. The mortar strength increases with the increase in the amount of NS sol. However, when it exceeds a certain amount, the growth effect is not obvious and there is a downward trend [28].

The pore structure has important effects on the properties of cement mortar and concrete and is especially closely related to the strength and transmission properties [29-31]. In the study of Han et al. [32], it was concluded that the correlation between the pore microstructural characteristics and mechanical properties was very strong. Porosity reduction and refinement of the pores in a cement paste increase the strength [33]. It is feasible to predict the performance of a cementitious material based on its pore structure characteristics [34].

Most of the studies intended to analyze the pore structure of cement-based materials by visual inspection, SEM, mercury intrusion porosimetry [33], 3D X-ray computed tomography (CT) [35], nuclear magnetic resonance (NMR) [36] and nitrogen adsorption-desorption measurement [37]. However, these methods have some shortcomings, for example, NMR and CT testing are complex and expensive [38], and each method has its own applicability. The measurement of pore structure analyzer (PSA) is a panoramic pore structure analysis method based on the optical microscope, and it is a widely recognized method for pore structure analysis. The collection of pores in the whole concrete cross-section by PSA is more suitable for the establishment of a strength quantitative model [42].

The improvement of pore structure in the microstructure by NS is one of the mechanisms for enhancing cement materials. In the result of Huang et al. [13], the incorporation of NS refined the pores and reduced the pore connectivity, which led to the improved sulfate resistance of cement mortars under partial immersion conditions. Feng et al. [23] found that NS particles successfully densify the pore structure, particularly leading to the reduction of large capillary pores. In the literature [39], the pore volume with a pore diameter greater than 10 µm accounts for the largest proportion, and the macropore was considered to be caused by the presence of entrapped air in the fresh paste during processing, which has not caused concern.

A review of all of the research conducted so far indicates that the effect of NS on the increase of micron-scale pores has not received attention. However, the increase in meso-porosity obviously has a great influence on the mechanical properties and durability of cement-based materials [40,41], which is an obstacle to the application of NS-modified cement-based materials.

To discuss the issues mentioned above, this article analyzes and models the effect of increased micropores encountered in the application of NS-modified cementbased materials, while building a bridge between the pores and strength. And this study aims to provide some information in terms of the research challenges encountered thus far. In particular, the correlation between mortar strength and micro-pore structure under the influence of NS sol was discussed by calculating the mortar matrix strength index.

2 Experimental

2.1 Raw materials

The NS sol, reference cement, natural river sand, and polycarboxylate superplasticizer (PS) were used as the raw materials. The NS sol was prepared using a simple silicon colloidal sol method, and the NS sol was directly mixed into the cement mortar as an admixture, the agglomeration of NS particles in cement was avoided because NS sol has favorable dispersion stability [42]. The SEM image of the NS particles in the NS sol is shown in Figure 1. The properties of the NS sol are shown in Table 1. Reference cement P.I 42.5 was used, and its main properties are listed in Table 2. Natural river sand was used as fine aggregate for the mortar. Its apparent density was 2,744 kg/m³, and its fineness modulus was 2.94. PS was provided by Sobute New Materials Co., Ltd. (Jiangsu, China), white powder.

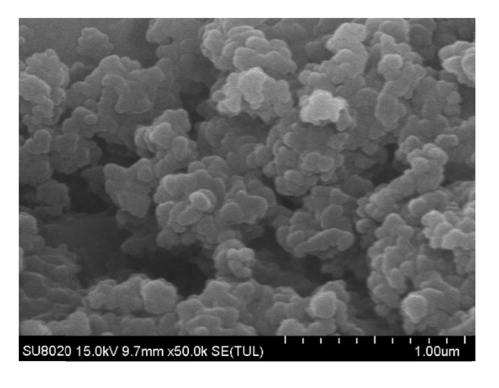


Figure 1: SEM image of NS particles precipitated by NS sol.

Table 1: Properties of NS sol

Appearance	Particle size (nm)	Content	рН	Solvent	Specific gravity	Specific surface area (cm²/g)	Viscosity (mPa s)
Translucent liquid	30	30%	7.9	Water	1.202	250 ± 30	3.39

Table 2: Properties of reference cement

Chemical composition	SiO ₂	Al ₂ O ₃	Fe ₂ O ₃	Ca0	MgO	Na ₂ O	SO ₃	Loss on ignition	Specific gravity	Specific surface (cm²/g)	Bulk density (g/cm ³)
Composition (%)	20.46	4.7	3.13	62.66	2.47	0.69	2.85	3.04	3.1	3520	1.75

2.2 Sample preparation

Three series of samples were prepared, including those with the NS contents of 1.5 and 3% of the cement by mass (S1 and S2) for the NS-modified mortar, and a control mortar (S0) for comparison. These samples used the same water/cement ratio of 0.5, as well as the same amounts of sand, cement, and PS. The mixed proportions of the different specimens are listed in Table 3. The sample preparation and strength examination of cement mortar tested were based on GB/T 17671-2020 (ISO 679) [43]. In three samples as a group, for each group of each series, the weight of the sand used was 1,350 g, the weight of the cement used was 450 g, the water consumption was 225 g, and the amount of PS was 1% of the cement. In addition, the NS content of the NS sol was 30%. Therefore, the NS sol consumption values for S1 and S2 groups were 22.5 and 45 g, respectively.

Four groups of mortars were made for each series, which were used for testing at the four ages of 3, 7, 14 and 28 days. Mortar prism specimens ($40 \text{ mm} \times 40 \text{ mm} \times 160 \text{ mm}$) were used to test the compressive and flexural strengths. First, water was mixed with NS sol and PS, added to the cement, and stirred for 30 s. Then, sand was added to the cement slurry, and stirring was continued for 210 s. After mixing and conducting a mortar

Table 3: Mix proportions of different specimens

Series	Sand (g)	Cement (g)	Water/cement	Admixture (g	
				NS sol	PS
S0	1,350	450	0.5	0	4.5
S1	1,350	450	0.5	22.5	4.5
S2	1,350	450	0.5	45	4.5

fluidity test, the fresh mortar was cast in molds, and a vibrator was used for compaction. The initial curing of the specimens was carried out in a standard curing chamber for concrete at a temperature of about 20°C and a relative humidity of about 95%. The mortar prism specimens were demolded after 48 h, placed in water, and cured in a standard curing room until tested.

2.3 Testing procedures

2.3.1 Mortar fluidity test

The fluidity test of the fresh mortar was performed in accordance with the standard "Test method of fluidity of cement mortar" (GB/T2419-2005) [44]. The newly mixed mortar was divided into two layers in a truncated cone round mold, and the mold sleeve was removed after tamping and pressing. After scraping off the excess mortar and smoothing it, the circular mold was lifted vertically from the truncated cone, and the mortar fluidity tester was turned on. After the tamping was completed, the maximum diffusion diameter of the bottom surface and its vertical diameter were measured with calipers, and the average value was calculated with an accuracy of 1 mm, which was the mortar fluidity.

2.3.2 Strength examination

The compressive and flexural strengths of the NS solmodified and control mortars at 3, 7, 14 and 28 days were tested. For each group, three samples were tested each time. The flexural strength was first tested using three-point loading, with a span of 120 mm and a loading rate of 0.06 mm/min. The broken mortar from the flexural

strength examination was used in the compressive strength examination. The compression loading area was $40 \times 40 \text{ mm}^2$, and the loading rate was 0.12 mm/min. A microcomputercontrolled universal tester was used for the compressive and flexural tests. It had a maximum load of 300 kN, and the error was $\pm 1\%$. It is worth noting that the strain rate of the compressive test is 5×10^{-5} s⁻¹, and the strain rate of the flexural test is 2.5×10^{-5} s⁻¹. Under this quasi-static loading test, the mortar strength obtained is relatively low [45].

2.3.3 Pore structure analysis

Pore structure analysis of the mortar was performed in accordance with the standard "Test code for hydraulic concrete" (SL/T 352-2020)[46]. A pore structure analyzer (PSA, Shanghai Lrel Instrument Co., Ltd, RapidAir) was used to determine the pore structure of the mortar. The linear traverse method was used. The test samples for the pore structure measurement were slices from the mortar broken in the flexural test at 28 days. The slice thickness was 15-20 mm. For each group, three center slices and three edge slices were used for the measurements. The observation area for the pore structure was a $30 \text{ mm} \times 30 \text{ mm}$ square in the middle of the slice. These mortar slices were ground and buffed using a burnisher before the pore structure measurements. The rotary speed of the burnisher was 50-60 rpm. The grinding time was 20 min, and the buffing time was 10 min.

Afterward, the slices were dried at 45°C for 3 h. A marker was used to color the surface of the mortar slices black, and white barium sulfate powder was dusted over the surface. After removing the excess powder, the mortar slices were placed in the PSA to observe the pores. Finally, the porosity and pore size distribution were calculated using a scanned binary image, with the pore structure values calculated according to the literature [47]. The process used in the pore structure measurement test is shown in Figure 2.

2.3.4 Microstructure observation

To understand and explain the NS modification mechanism, the microstructure of the NS-modified cement hydration products was determined using SEM. An ultrahigh-resolution field SEM (ZEIZZ EVO, Carl Zeiss AG, Germany) was used to analyze the microstructure of the samples. A mortar specimen was broken to obtain pieces with a volume of <1 cm³, as shown in Figure 3, which were placed in alcohol as SEM observation samples. Small fractured samples at every hydration age were soaked in anhydrous ethanol to stop hydration and dried at 50°C for 12 h. Before the SEM observations, the mortar specimens were dried at 45°C, and the surface was sprayed with gold powder using sputtering.

A general overview of the experimental program is shown in Figure 4; the key parameters of all tests and the type and number of specimens are provided.

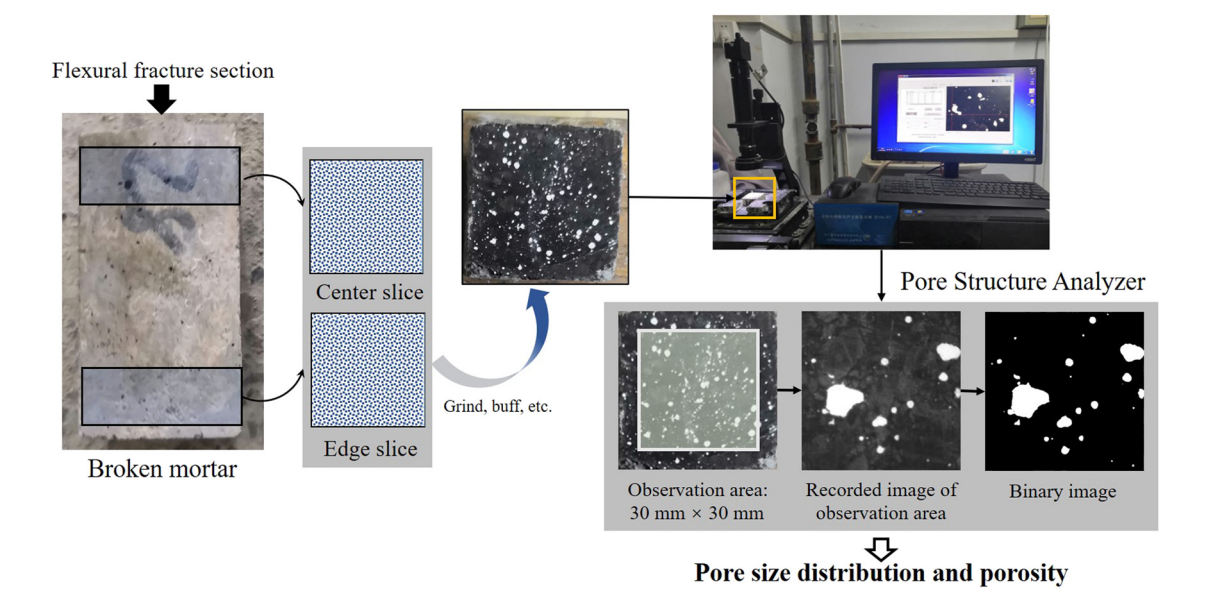


Figure 2: Pore structure measurement.



Figure 3: SEM micro-samples.

3 Theoretical relationship model between pore structure and strength

The porosity and pore size distribution significantly affect the capabilities of numerous materials. In particular, they are closely related to the strength of cement mortar [48]. Many scholars have established equations for quantitatively researching the pore structure and strength [49-51]. In this study, cement mortar consists of fine aggregate, cement paste and pores. The proportion of aggregate in the mortar is very large, in order to avoid a huge amount of calculation aggregate; aggregate and cement paste are unified into a mortar matrix. The cement mortar was equivalent to a two-phase composite composed of the mortar matrix and pores. The mortar matrix strength index values of mortar specimens S0, S1 and S2 were derived based on the strength test and pore structure measurement results for the NS sol-modified mortar. The calculation method reported by Luping [51] and Jin et al. [52] was referenced.

The parallel porous body model was used to research the pore structure and strength quantitatively, and to determine the effect of the pore size distribution. In addition, the pores were simplified to round shapes in the two-dimensional model. The equivalent relationship between the two models is shown in Figure 5. The two-phase model is equivalent to a calculation model composed of n porous bodies. In each porous body, the pores are considered to have a consistent size, where r_n is the pore size of the nth porous body, and the nth porous body is represented by B_n .

For the two-phase model, the relationship between porosity v and effective area ratio A_m can be calculated using equation (1). According to Griffith's theory, the critical stress, σ_c , when the porous body fractures can be expressed as equation (2), where K indicates the strength of the mortar matrix. The deduction of K is based on references [51,52]. It is defined as the matrix strength index in this article.

$$A_m = 1 - \pi^{1/3} \left(\frac{3}{4}v\right)^{2/3},\tag{1}$$

$$\sigma_{\rm c} = \sqrt{KA_m/r} \,. \tag{2}$$

For the parallel model, during the compressive loading of the mortar, the force of each porous body gradually increases, and the effective area of B_1 with the largest radius r_1 has the smallest value. When B_1 is destroyed, there is a correlation between nominal stress σ , load P_1 , and matrix strength index K, as shown in equation (3), and the effective area ratio would increase from A_{m1} to A_{m2} equation (4). Moreover, the steps are repeated until all the porous bodies are damaged, and theoretical strength f_c can be calculated according to equation (5).

$$\sigma = P_1/A_{m1} > \sqrt{KA_{m1}/r_1},$$
 (3)

$$A_{m2} = A_{m1} \left(1 - \frac{V_1}{V} \right), \tag{4}$$

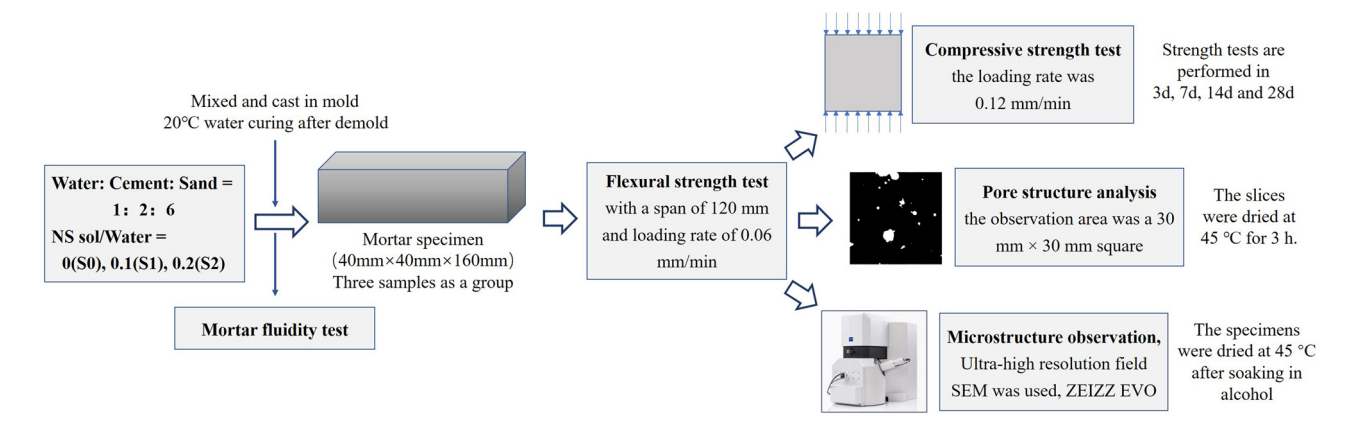


Figure 4: General overview of the experimental program.

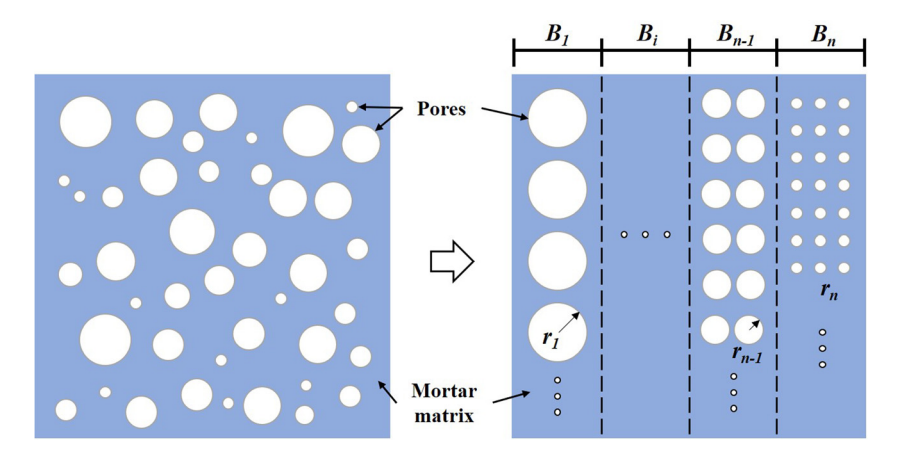


Figure 5: Equivalence of two-phase round pore model and parallel porous body model [48].

$$f_{\rm c} = \sigma = P/A_{mn} > \sqrt{KA_{mn}/r_n}$$
 (5)

Matrix strength index *K* is difficult to obtain through experiments. In this study, experimental data and a computer program were used to determine *K*. Furthermore, a quantitative study of the pore structure and strength of the NS sol-modified mortar was performed based on the test results and calculation results.

4 Results and discussion

4.1 Mortar fluidity

Each group of mortar fluidity values of S0, S1 and S2 are shown in Figure 6. These results indicated that the mortar fluidity decreased as the NS content increased. At NS contents of 1.5 and 3%, the mortar fluidity was

considerably reduced. Relative to S0, the mortar fluidity was reduced by 16.3 and 36.9% with NS contents of 1.5 and 3%, respectively. Clearly, the addition of NS sol was detrimental to the workability of the mortar.

The negative impact of NS on the workability of cementitious materials has been recognized [53,54]. It is due to the fact that the surfaces of NS particles have a powerful attraction and high specific surface area, which allow them to adsorb water molecules in the mixing water on their surfaces. Thus, the reduced free water in the fresh cement mortar leads to reduced mortar fluidity [23].

4.2 Mortar strength

The compressive strengths of the NS-modified mortar (S1 and S2) and control mortar (S0) are shown in Figure 7.

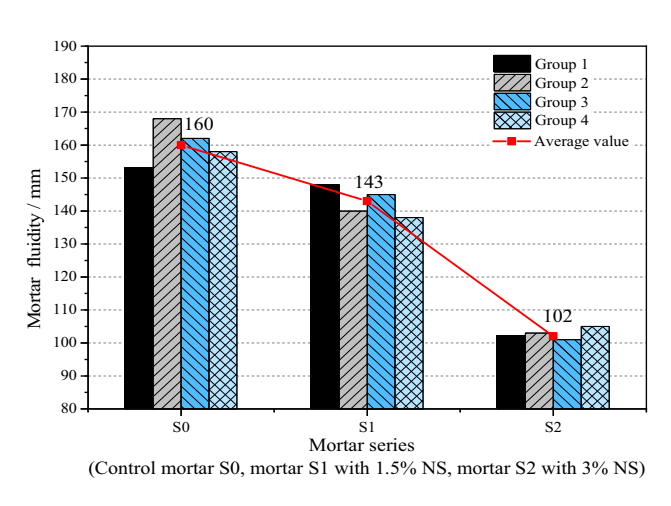


Figure 6: Mortar fluidity test results.

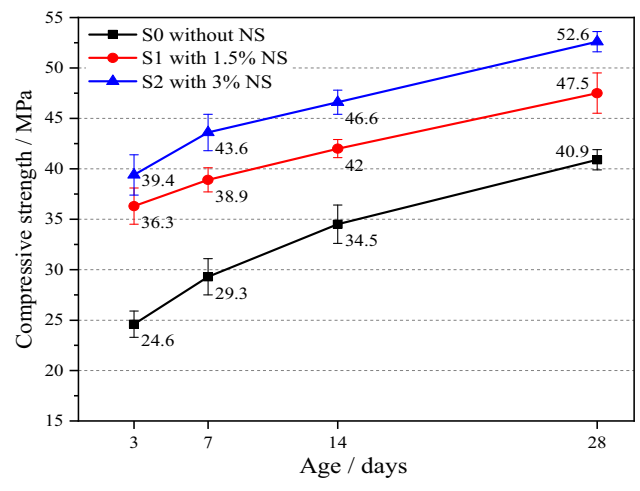


Figure 7: Development of compressive strength.

The compressive strength test results indicated that mixing NS sol into the mortar increased its compressive strength. Compared to S0, the compressive strength of S1 was increased by 47.6% at 3 days, 32.8% at 7 days, 21.7% at 14 days, and 16.1% at 28 days. The compressive strength of S2 was increased by 60.2% at 3 days, 48.8% at 7 days, 35.1% at 14 days, and 28.6% at 28 days. The compressive strength of the mortar mixed with NS sol was significantly improved.

The flexural strengths of the NS-modified mortars (S1 and S2) and control mortar (S0) are shown in Figure 8. Consistent with the compressive strength test results, the flexural strength increased when the NS sol was mixed into the mortar. Compared to S0, the flexural strength of S1 was increased by 22.6% at 3 days, 19.3% at 7 days, 12.8% at 14 days, and 6.5% at 28 days. The flexural strength of S2 was increased by 32.5% at 3 days, 27.8% at 7 days, 15.9% at 14 days, and 10.7% at 28 days. Likewise, when the NS sol dosage was increased, the improvement in the flexural strength was more obvious.

As the age increased, the compressive and flexural strength enhancement effects decreased. Clearly, the NS sol had a greater effect on the early compressive strength of the mortar. At 3 days, the compressive strength enhancement effect of 3% NS was more than 60%, and the effect of 1.5% NS was more than 45%. In addition, the NS modification had a smaller enhancement effect on the flexural strength than on the compressive strength. This showed that NS had no significant enhancement effect on the mortar toughness.

The test results for the mortar mechanical properties indicated that the cement mortar strength was enhanced by the modification with the NS sol, with a more significant

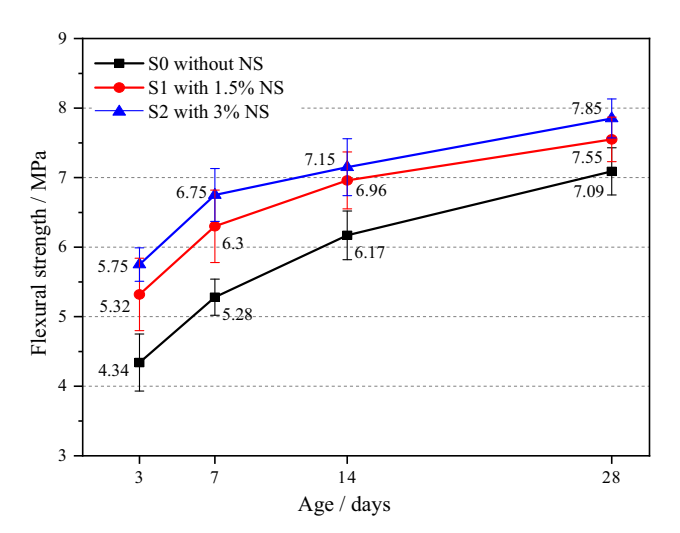


Figure 8: Development of flexural strength.

enhancement effect on the early (3 and 7 days) strength. NS has greater pozzolanic activity than silica fume [12], which meanwhile promotes the hydration process inside the cement matrix. Therefore, the NS had an excellent enhancement effect on the early strength of the mortar. Moreover, the microstructure of the cement matrix could be enhanced by the filling effect, where nanoscale silica particles in the NS sol filled the micro-nano-pores in the cementitious material. Thus, the microstructure of the NS-modified cementitious material was denser, and the performance was excellent.

4.3 Pore structure

Binary images of the pore distributions of samples S0, S1, and S2 are shown as Figure 9, in which the white areas indicate the pores, and the black area is the mortar matrix. It is obvious that the shape and distribution of the pores in the edge and center slices are consistent, and the number of pores increases with an increase in the NS sol dosage.

The porosity values were calculated for center and edge slices of S0, S1, and S2, which are shown in Figure 10. A comparison of the porosities of the center and edge slices of S0 and S1 shows that there is not much difference. The porosities of S2 were 11.92% (center slice) and 10.35% (edge slice). Thus, the porosity of the center slice was 15% greater than that of the edge slice. Based on the average porosity of the center and edge slice, the porosities of S1 and S2 were 26.5 and 72.3% greater than that of S0, respectively. Undoubtedly, as the NS content increased, the mortar porosity increased.

The pore size distributions and corresponding porosities are shown in Figure 11(a) and (b). These results indicate that the pore size distribution trends for all samples were almost identical. In the pore radius range of 1–50 μ m, as the pore size increases, the corresponding porosity increases. The corresponding porosity fluctuates in the pore radius range of 50–300 μ m. The corresponding porosity finally peaks in the pore radius range of 300–1,000 μ m. The peak porosity of the center slice was 1.75–2%, and the peak porosity of the edge slice was 1.75–3%. S2 edge slices had the highest peak porosity of 2.9%. In addition, the radii of the pores tested in the S0 and S2 slices hardly exceeded 1,000 μ m, whereas the radii of some pores in the S2 center and edge slices tested were larger than 1,000 μ m.

The cumulative porosity curves of the six test slices are shown in Figure 12(a)-(c). For samples S0 and S1, the

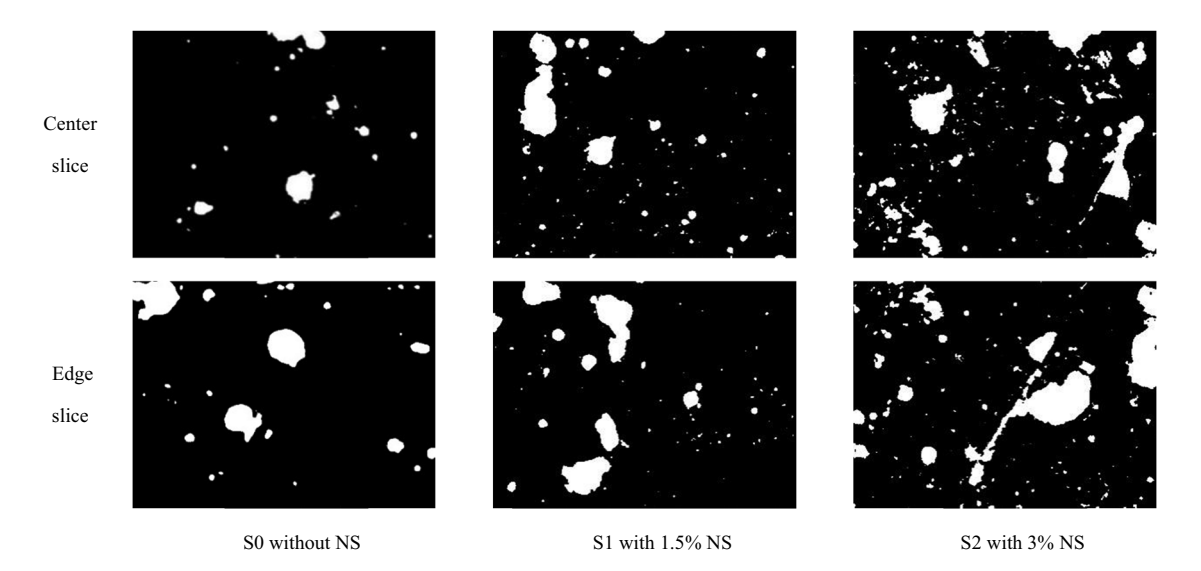
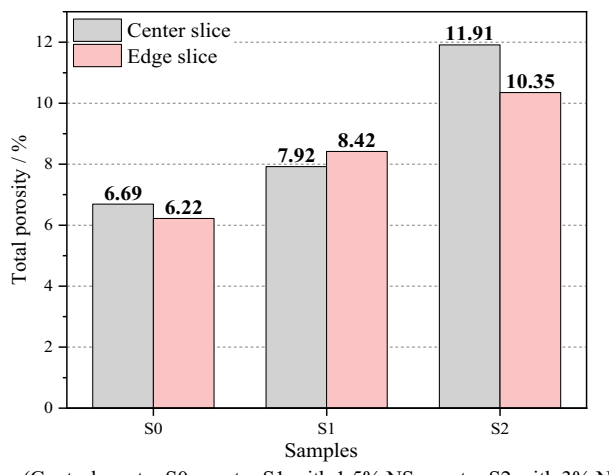


Figure 9: Binary images of sample pore distributions.



(Control mortar S0, mortar S1 with 1.5% NS, mortar S2 with 3% NS)

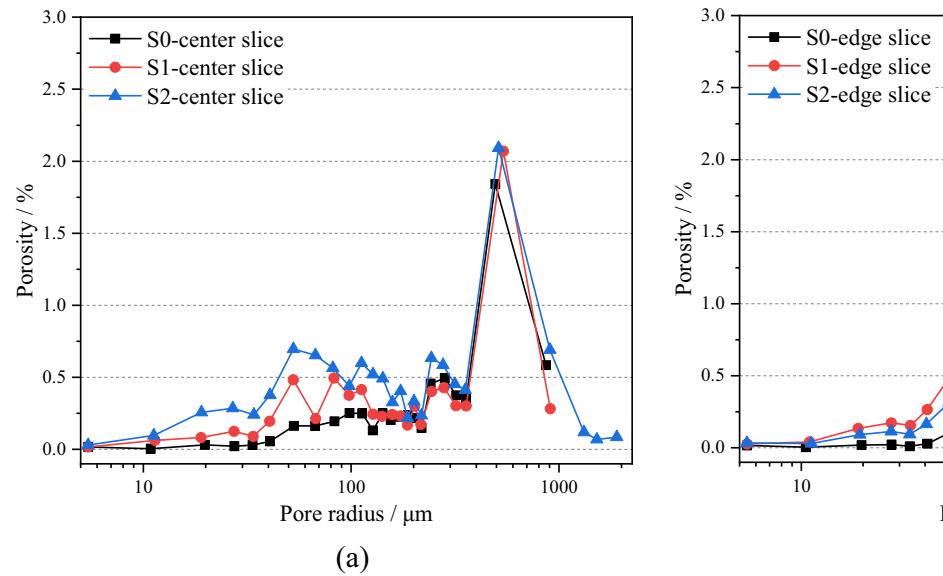
Figure 10: Total porosity of hardened mortar.

trends for the curves of the edge and center slices are consistent, whereas the curves of the edge and center slices of sample S2 are very different. In Figure 12(a), the cumulative porosity percentage of the 100 μm pores is approximately 10%, whereas, in Figure 12(b), the cumulative porosity percentage of the 100 μm pores is approximately 30%. These results show that the number of micropores (1–100 μm) in sample S1 was greater than those in S0. In Figure 12(c), at the 100 μm pore size, the cumulative porosity percentage of the S2 center slice is approximately 30%, and that of the S2 edge slice is approximately 18%. In addition, the total porosity of S2 is 10–12%, which indicates that there was a greater number of micropores (1–100 μm) and macropores (>100 μm) in the S2 sample.

In summary, the porosity increased with the NS sol dosage. This result was consistent with the results reported by Feng et al. [23]. When the content of large capillary pores (0.05–10 µm) in an NS sample was higher than expected, they suggested that the density of NS hydration products led to their diffusion being hindered, which produced more pore structures [55]. The porosity and pore distribution were investigated using the linear traverse method. Compared with the reference sample, there was an increase in the number of micropores with radii of 1-100 µm in the mortar sample with a dosage of 1.5% NS, whereas both the micropores (1–100 µm) and macropores (>100 µm) increased in the mortar sample with the dosage of 3% NS. The pore structure has significant effects on the mechanical properties of mortar and other cementitious materials [56]. In this study, the relationship between the pore structure and strength of the NS sol-modified cement mortar was investigated using theoretical calculations.

4.4 SEM results

Figure 13 shows microstructure images of three hardened mortar samples. The microstructure of the C-S-H gel of the three group specimens is critically different, and the difference in compactness is resulting from the shape and size of the particles. In the control mortar, Figure 13(a) and (b), hydrated cement paste is an accumulation composed of angular particles typically in the size range from 50 to 200 nm. It can be seen that the reference sample has a relatively loose



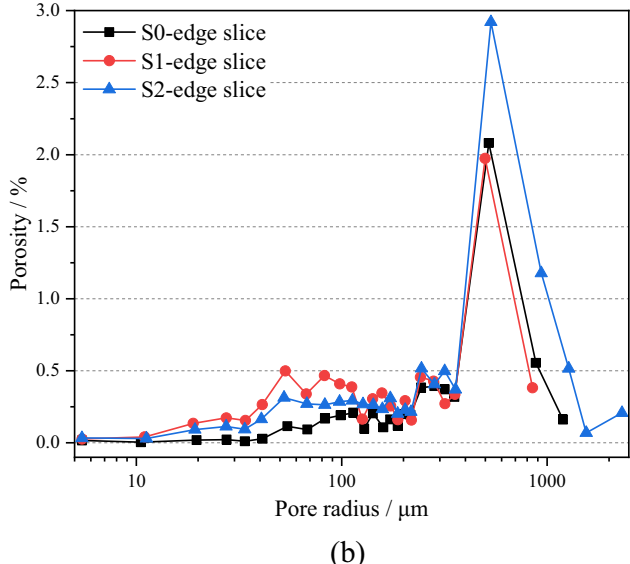


Figure 11: Pore size distributions: (a) center slice and (b) edge slice.

microstructure with a number of large voids as marked in the image.

In the microstructure of S1, Figure 13(c) and (d), there are spherical particles with a size of 100-200 nm distributed on the hardened cement paste, and the cement paste is composed of some dense layered structures; C-S-H spherical particles were formed on the surface of hydration products. In the microstructure of S2, Figure 13(e) and (f), hardened cement paste is almost entirely composed of layered structures, and there is a reticular network shape. As shown in images (d) and (f), both the S1 and S2 were able to densify the microstructure and the proportion of capillary pores is significantly reduced, as indicated by the vellow circles. It is obvious that the influence of the higher dosage of NS on the microscopic morphology of C-S-H is significant, the effect of NS on the crystal morphology of C-S-H causes the refinement of interlayer pores, which is the key to improving the strength of mortar. These results were close to those reported by Feng et al. [23] and Hou et al. [26,55]. In addition, the setting time of NS concrete is shortened, the slump is reduced, and the shrinkage is improved owing to the high activity and nucleation of NS [57]. In summary, the incorporation of NS significantly improved the microscopic properties of NS-modified cement mortar.

4.5 Calculation and result analysis

Because of the high specific surface ratio, the free dispersed water in the mixture existing among the particles

of cement and NS will be decreased by the high specific surface ratio of the nanoparticle. As a result, the addition of NS into the mortar can greatly change the properties of the fresh mortar [15], this change will lead to the increase of mesoscopic pores (micron-scale pores) [23]. Although NS enhances the strength of mortar, the increase in micron porosity may be a critical issue in the application of NS-modified mortar. Therefore, the quantitative relationship between micron porosity and strength under the influence of NS is calculated, and this research reveals the effect of NS limited by micropores on the strength of mortar.

The strength, porosity, and pore size distribution of the NS sol-modified and control mortars were measured in the previously discussed experiments. In the calculation, the measured pores were subdivided into six size ranges according to the pore radii: <50, 50-100, 100-200, 200-500, 500-1,000, and >1,000 μm. In addition, because the pore structure distribution results were from six mortar slices, the relationship between the pore structure and strength in each of the three mortar groups was calculated using the center and edge slices. The parameters used for the quantitative calculations for the six mortar slices are listed in Table 4, where r_i is the average pore size, V_i is the porosity, V is the total porosity, and f_c is the compressive strength. The matrix strength index, K, values of the NS sol-modified mortar and control mortar were calculated using equations (1)-(5), the compiled computer program, and the calculation parameters from the strength test and pore structure measurement. The K value has been

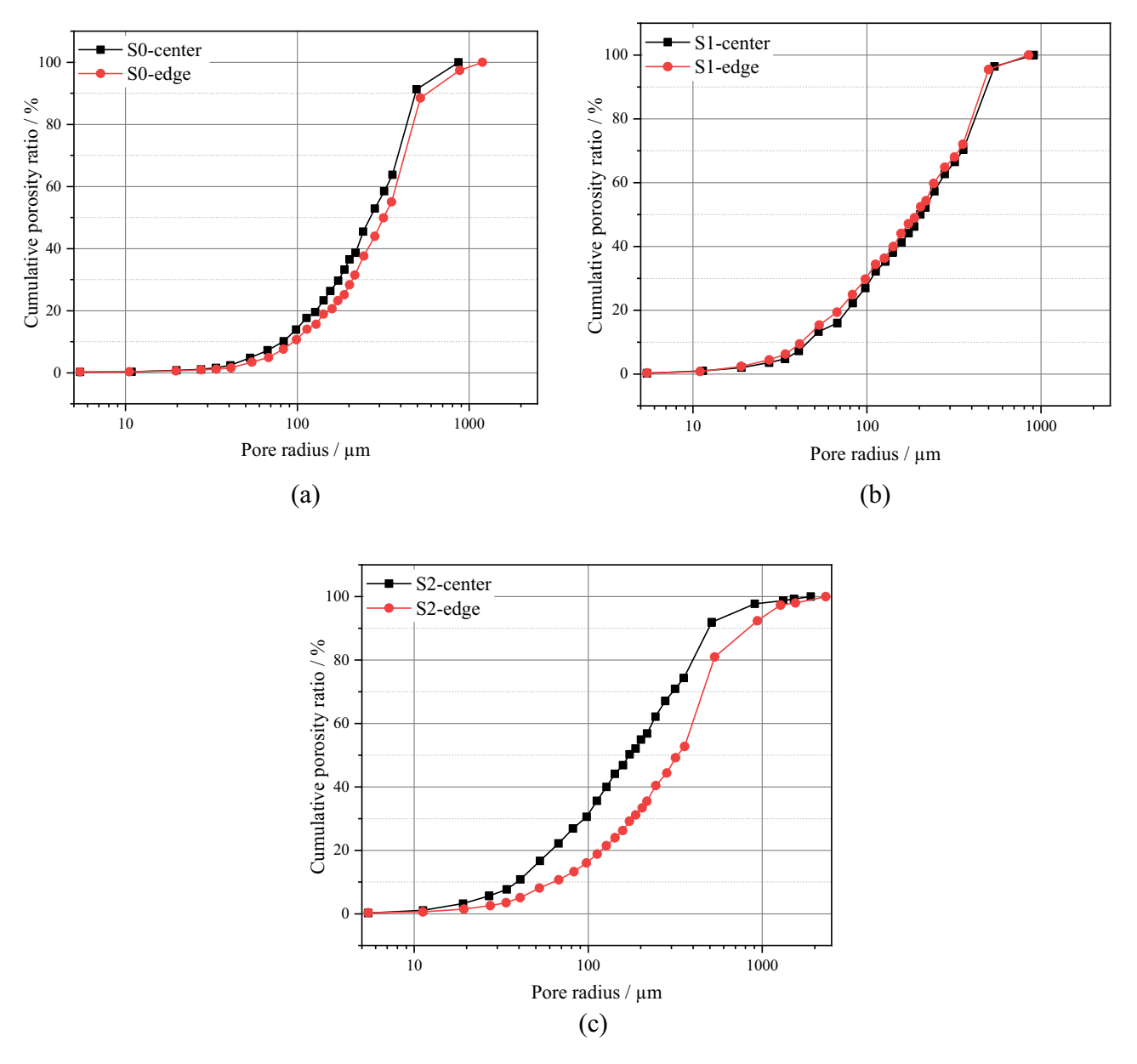


Figure 12: Cumulative porosity ratio of test samples: (a) S0 without NS, (b) S1 with 1.5% NS, and (c) S2 S1 with 3% NS.

repeatedly calculated, and the results show that K is a constant related to pore distribution and strength.

In the calculation, the preliminary range of K was determined through a trial calculation, where K was an integer from 1 to 7. Then, the corresponding compressive strength was calculated. The K-compressive strength correlation curves of the six mortar slices were obtained and are shown in Figure 14 (a) and (b). The compressive strength had an obvious positive linear correlation with matrix strength index K. In general, the linear intercepts of all the K-compressive strength correlation curves were in the range of 0.3–0.5, which showed that there

was little difference. Thus, the linear intercept was ignored in this study. The slope of the K-compressive strength correlation curve was used to represent the ratio of compressive strength f_c to matrix strength index K. For many materials, there is a curvilinear relationship between a and the porosity. The relationship between the f_c/K and total porosity values of the tested slices is shown in Figure 15. The primary issue can be summarized as follows: when the porosity increases, the curve slopes decrease. It was obvious that an increase in porosity decreased the strength of the mortar. In addition, the trend for the NS sol-modification effect was a curvilinear

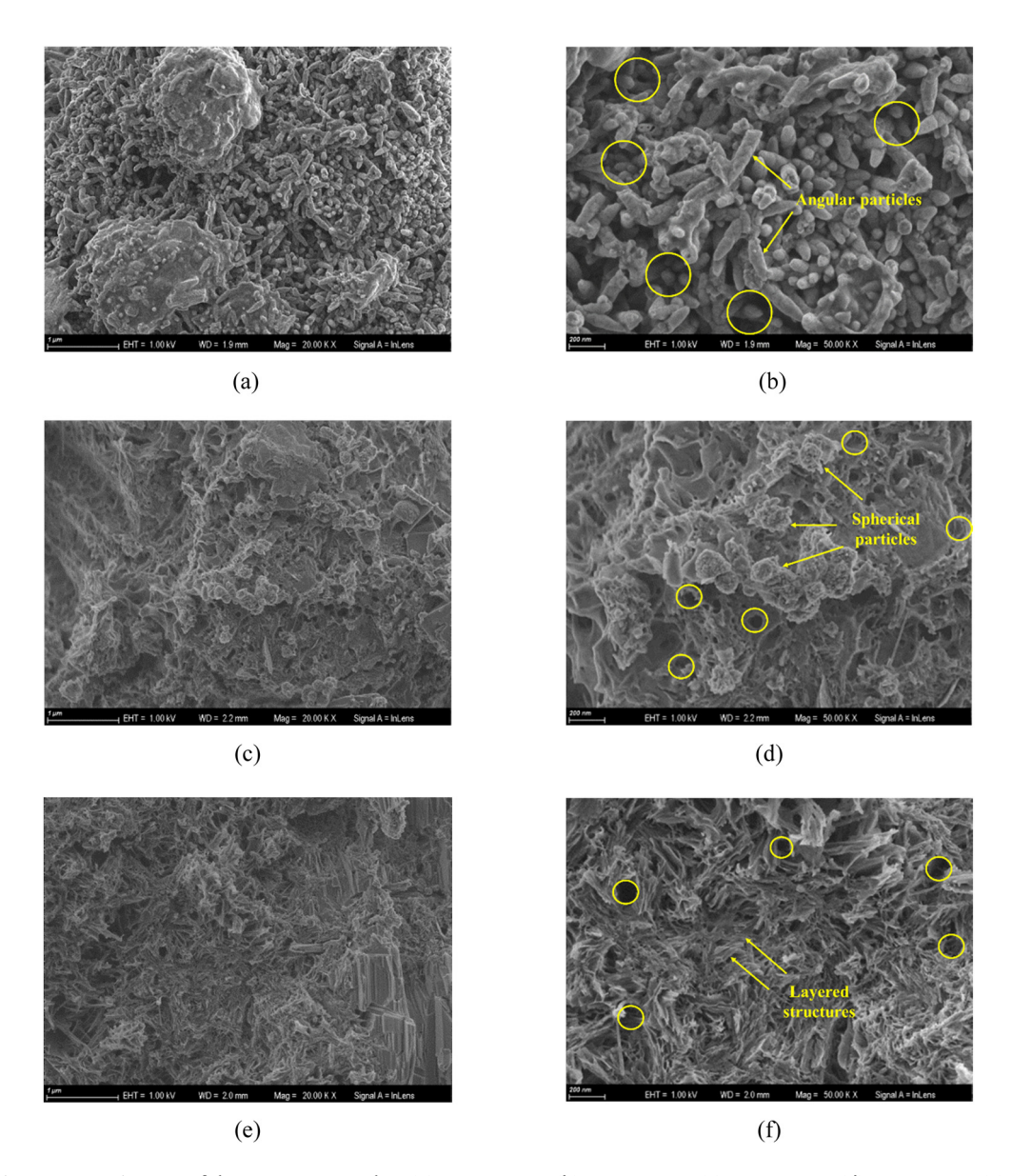


Figure 13: Microstructure images of three mortar samples. (a) S0 20,000 \times , (b) S0 50,000 \times , (c) S1 20,000 \times , (d) S1 50,000 \times , (e) S2 20,000 \times , and (f) S2 50,000 \times .

Table 4: Parameters for quantitative calculations

Size range	S0-center		S0-edge		S1-center		S1-edge		S2-center		S2-edge	
	r _i (μm)	V _i (%)	r _i (μm)	V _i (%)	r _i (μm)	V _i (%)	r _i (μm)	V _i (%)	<i>r_i</i> (μm)	V _i (%)	r _i (μm)	V _i (%)
<50	19.6	0.16	16.5	0.10	26.4	0.57	24.1	0.79	23.6	1.29	21.4	0.53
50-100	74.3	0.77	76.2	0.57	75.6	1.56	70.6	1.71	68.6	2.36	70.4	1.13
100-200	146.1	1.29	142.9	0.90	152.3	1.53	141.3	1.62	138.7	2.56	143.8	1.57
200-500	344.6	3.89	268.5	1.86	365.7	1.91	345.7	3.91	263.8	2.65	270.3	2.23
500-1,000	866.4	0.58	569.4	2.64	863.2	2.35	849.7	0.38	573.8	2.78	608.3	4.10
>1,000	None		1194.7	0.16	None		None		1514.9	0.27	1471.0	0.79
V (%)	6.69		6.22		7.92		8.42		11.91		10.35	
f_{c} (MPa)	40.9				47.5				52.6			

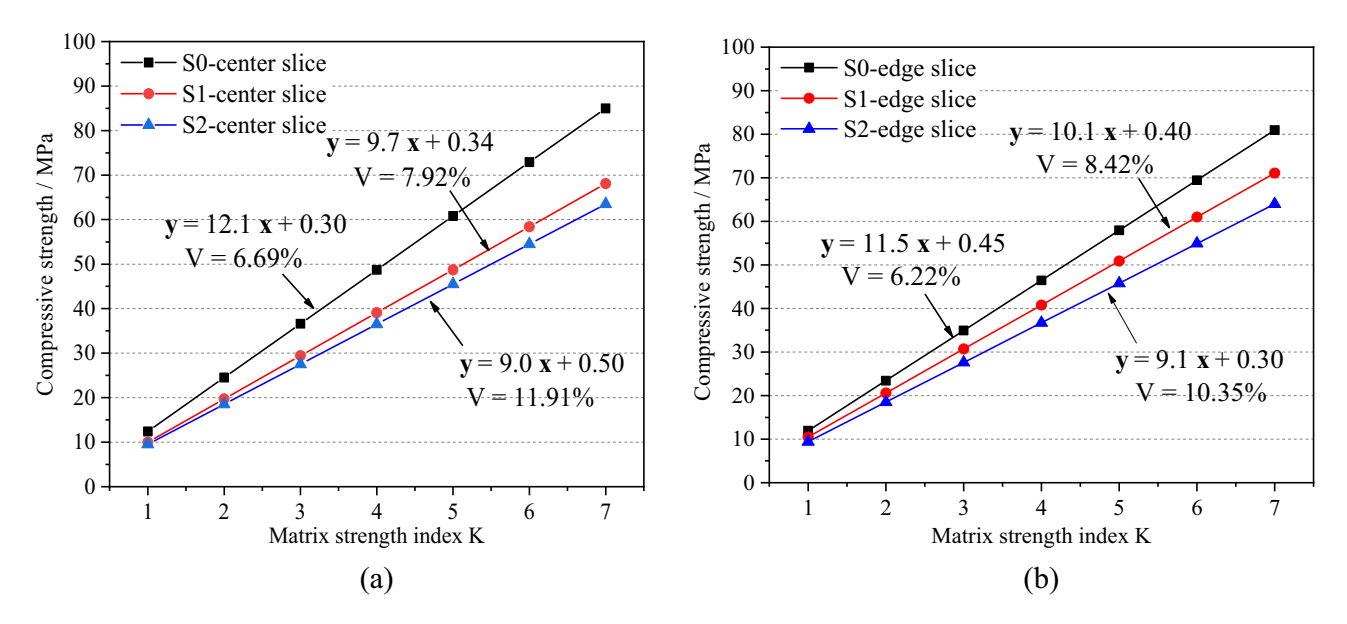


Figure 14: Relationship between K and compressive strength. (a) Center slice and (b) edge slice.

relationship, which indicated that the strength of the NS-modified mortar would be greater if the porosity of the three groups was consistent.

The measured compression strengths of mortar specimens S0, S1, and S2 were 40.9, 47.5, and 52.6 MPa, respectively. In addition to the K-compressive strength curves, the values of the matrix strength index S0, S1, and S2 were 3.52-3.85, 4.66-4.87, and 5.75-5.79, respectively. This study further showed that the effect of the NS sol on the mortar matrix strength became more significant when the amount of NS sol increased.

The trends for the total porosity, compressive strength, and matrix strength index *K* are shown in Figure 16. It was found that the total porosity, compressive strength, and matrix strength increased with an increase in the NS sol dosage. In general, the porosity and strength of solid materials have an inverse relationship, and the strength depends on the solid part of the material. Hu et al. [48] studied the porosity and strength of carbon nanotubemodified mortar and found that a large increase in porosity led to a decrease in mortar strength. In this study, it was obvious that the increase in porosity was not sufficient

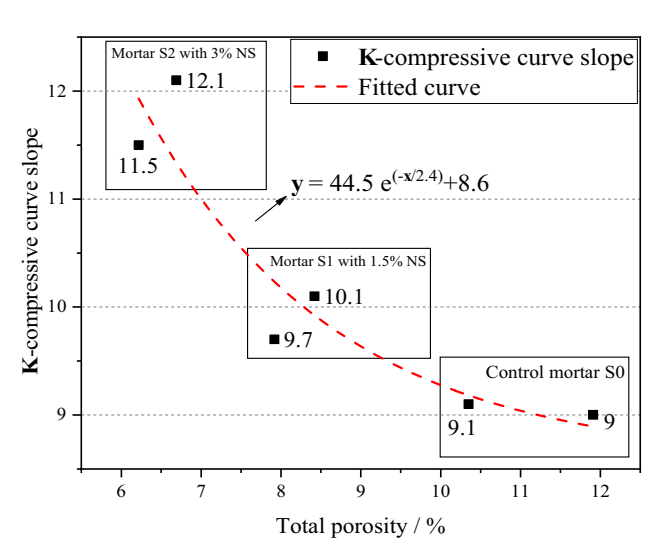


Figure 15: Trend of mortar/matrix strength ratio.

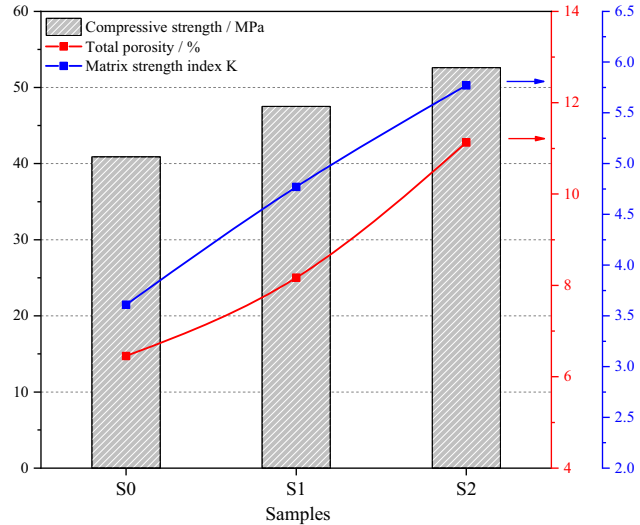


Figure 16: Trend curves of compressive strength, total porosity, and matrix strength index K.

to affect the mortar strength negatively. By contrast, with NS contents of 1.5 and 3%, the compressive strength was enhanced by 16.1 and 28.6%, respectively, and *K* increased by 29.3 and 56.6%, respectively. The results suggested that the increase in the strength of the NS-modified mortar was limited by the increase in porosity.

5 Conclusion

This study focused on the quantitative relationship between the pore structure and strength of this NS sol-modified mortar. The pore structure distribution is analyzed using PSA, and the microstructure of the modified mortar was investigated using SEM; the fluidity and strength of mortar are also studied. Based on the above tests, a theoretical calculation of the relationship between the strength and pore structure was performed. The main conclusions of the research can be summarized as follows:

- 1) It was found that NS sol increased the porous structure in the modified mortar. Relative to the control mortar, with NS contents of 1.5 and 3%, the porosity was increased by 26.5 and 72.3%, respectively. The micropores (1–100 μ m) in the mortar sample with the 1.5% NS dosage were increased, while the micropores (1–100 μ m) and macropores (>100 μ m) of the mortar sample with the 3% NS dosage were both increased.
- 2) The morphology of the hydration products of mortar cement changes with the increase of NS sol content. In the NS sol-modified mortar, C–S–H spherical particles were formed on the surface of hydration products, and the effect of NS on the crystal morphology of C–S–H causes the refinement of pores, which reflects the influence of the high pozzolanic activity and filling effect of NS in the process of cement hydration. The effect of NS on the microstructure of cement mortar is the mechanism of strength improvement.
- 3) NS significantly improved the matrix strength of the mortar, and the ratio of the mortar strength to matrix strength showed a negative correlation with the increase in porosity. The mortar matrix strength index, *K*, was calculated using a simplified theoretical model. The slope of the *K*-compressive strength curve decreased with increasing porosity, which meant that the ratio of the compressive strength to the mortar matrix strength was affected by the porosity. With NS contents of 1.5 and 3%, *K* was increased by 29.3 and 56.6%, respectively.

4) The relationship between the strength and pore structure was discussed. This research showed that the mechanical properties, matrix strength, and porosity of the NS sol-modified mortar were improved. Calculation results showed that the increase in porosity was unfavorable for an increase in the mortar strength, and the enhancement effect of NS on the mortar matrix is greater than the reduction effect of increasing porosity on the strength.

In summary, the quantitative relationship between the micron-scale pores and strength of NS sol-modified mortar was studied and discussed. More research studies should be conducted on the pore size distribution for digging into the durability evolution mechanism.

Funding information: The authors would like to acknowledge the financial support received from the National Natural Science Foundation of China (Grant No. 52179145, U2040224, 52130901), Scientific and Technological Research Project in Henan province (Grant No.222300420081), the Program for Science and Technology Innovation Talents in Universities of Henan Province (21HASTIT013), and Open Research Fund Program of State key Laboratory of Hydroscience and Engineering (sklhse-2022-c-01).

Author contributions: All authors have accepted responsibility for the entire content of this manuscript and approved its submission.

Conflict of interest: The authors state no conflict of interest.

Data availability statement: The data that support the findings of this study are available from the corresponding author, [J.W.], upon reasonable request.

References

- [1] Yoo DY, Oh T, Kang MC, Kim MJ, Choi H-J. Enhanced tensile ductility and sustainability of high-strength strain-hardening cementitious composites using waste cement kiln dust and oxidized polyethylene fibers. Cem Concr Comp. 2021;120:104030.
- [2] Kolawole JT, Babafemi AJ, Fanijo E, Chandra Paul S, Combrinck R. State-of-the-art review on the use of sugarcane bagasse ash in cementitious materials. Cem Concr Comp. 2021;118:103975.
- [3] Gao Z, Zhang P, Wang J, Wang K, Zhang T. Interfacial properties of geopolymer mortar and concrete substrate: Effect of

- polyvinyl alcohol fiber and nano-SiO2 contents. Constr Build Mater. 2022;315:125735.
- [4] Oh JA, Zhuge Y, Araby S, Wang R, Yu H, Fan W, et al. Cement nanocomposites containing montmorillonite nanosheets modified with surfactants of various chain lengths. Cem Concr Comp. 2021;116:103894.
- Wang J, Xu Y, Wu X, Zhang P, Hu S. Advances of graphene- and graphene oxide-modified cementitious materials. Nanotechnol Rev. 2020;9(1):465-77.
- Mu S, Yue J, Wang Y, Feng C. Electrical, piezoresistive and electromagnetic properties of graphene reinforced cement composites: a review. Nanomaterials. 2021;11(12):3220.
- Abhilash PP, Nayak DK, Sangoju B, Kumar R, Kumar V. Effect of nano-silica in concrete; a review. Constr Build Mater. 2021-278
- [8] Liu C, He X, Deng X, Wu Y, Zheng Z, Liu J, et al. Application of nanomaterials in ultra-high performance concrete: A review. Nanotechnol Rev. 2020;9(1):1427-44.
- Ren Z, Liu Y, Yuan L, Luan C, Wang J, Cheng X, et al. Optimizing the content of nano-SiO₂, nano-TiO₂ and nano-CaCO₃ in Portland cement paste by response surface methodology. J Build Eng. 2021;35:102073.
- [10] Xu J, Wang B, Zuo J. Modification effects of nanosilica on the interfacial transition zone in concrete: A multiscale approach. Cem Concr Comp. 2017;81:1-10.
- [11] Stefanidou M, Papayianni I. Influence of nano-SiO₂ on the Portland cement pastes. Compos Part B-Eng. 2012;43(6):2706-10.
- [12] Byung-Wan J, Chang-Hyun K, Ghi-ho T, Jong-Bin P. Characteristics of cement mortar with nano-SiO₂ particles. Constr Build Mater. 2007;21(6):1351-5.
- [13] Huang Q, Zhu X, Zhao L, Zhao M, Liu Y, Zeng X. Effect of nanosilica on sulfate resistance of cement mortar under partial immersion. Constr Build Mater. 2020;231:117180.
- [14] Zhang M, Li H. Pore structure and chloride permeability of concrete containing nano-particles for pavement. Constr Build Mater. 2011;25(2):608-16.
- [15] Zhang P, Wan J, Wang K, Li Q. Influence of nano-SiO₂ on properties of fresh and hardened high performance concrete: A state-of-the-art review. Constr Build Mater. 2017:148:648-58.
- [16] Yang J, She W, Zuo W, Lyu K, Zhang Q. Rational application of nano-SiO₂ in cement paste incorporated with silane: Counterbalancing and synergistic effects. Cem Concr Comp. 2021;118:103959.
- [17] Zhao Z, Kong J, Yang H. Study on frost resistance of nano SiO₂ cement concrete. Appl Mech Mater. 2012;198-199:48-51.
- [18] Yu W, Sun L, Wu C, Shao C. Study for frost resistance of cement concrete pavement with NanoSiO₂ as admixture. Adv Mater Res. 2014;952:47-50.
- [19] Supit SWM, Shaikh FUA. Durability properties of high volume fly ash concrete containing nano-silica. Mater Struct. 2014;48:2431-45.
- [20] Zhang P, Zhang H, Cui G, Yue X, Guo J, Hui D. Effect of steel fiber on impact resistance and durability of concrete containing nano-SiO₂. Nanotechnol Rev. 2021;10(1):504-17.
- [21] Li G, Ding Y, Gao TY, Qin YM, Lv YJ, Wang KJ. Chloride resistance of concrete containing nanoparticle-modified polymer cementitious coatings. Constr Build Mater. 2021;14:299.

- [22] Liu X, Feng P, Shu X, Ran Q. Effects of highly dispersed nano-SiO₂ on the microstructure development of cement pastes. Mater Struct. 2019;53(1):1-4.
- [23] Feng P, Chang H, Liu X, Ye S, Shu X, Ran Q. The significance of dispersion of nano-SiO2 on early age hydration of cement pastes. Mater Des. 2020;186:108320.
- [24] Dongya Y, Qiu F, Fullong Z, Dongmei W, Qingin Z. Preparation and characterization of nano CaCO₃ modified with silica sol and study of its property. Rare Met Mat Eng. 2008;37:351-4.
- [25] Yao Y-C, Tseng S-T, Wong DSH. Shelf-life prediction of nanosol via pH acceleration. J Qual Technol. 2017;49(1):46-63.
- [26] Hou P, Kawashima S, Kong D, Corr DJ, Qian J, Shah SP. Modification effects of colloidal nanoSiO₂ on cement hydration and its gel property. Compos Part B-Eng. 2013;45(1):440-8.
- [27] Flores I, Sobolev K, Torres-Martinez LM, Cuellar EL, Valdez PL, Zarazua E. Performance of cement systems with nano-SiO₂ particles produced by using the sol-gel method. Transp Res Rec. 2010;2141(1):10-4.
- [28] Zhang X, Song X, Gao R. Effect of nano-silica sol on mechanical properties of cement mortar and the action mechanism. B Chin Ceram Soc. 2014;33:589-92.
- Gao M, Xiao J, Zuo S. Multifractal analysis on pore structure of [29] cement-based materials blended with ground limestone and its relationship with permeability. J Chin Ceram Soc. 2019;47:617-24.
- Elgalhud AA, Dhir R, Ghataora G. Limestone addition effects on concrete porosity. Cem Concr Comp. 2016;72:222-34.
- Wang B, Zhao R, Zhang T. Pore structure and durability of cement-based composites doped with graphene nanoplatelets. Mater Exp. 2018;8:149-56.
- [32] Han TS, Zhang X, Kim JS, Chung SY, Lim JH, Linder C. Area of lineal-path function for describing the pore microstructures of cement paste and their relations to the mechanical properties simulated from μ -CT microstructures. Cem Concr Compos. 2018;89:1-17.
- [33] Jambor J. Pore structure and strength development of cement composites. Cem Concr Res. 1990;20(6):948-54.
- Guo Y, Zhang T, Liu X, Tian W, Chen P, Wei J, et al. The pore fillability of cementitious materials and its application in predicting compressive strength of gap-graded blended cements. Constr Build Mater. 2018;168:805-17.
- [35] Shields Y, Garboczi E, Weiss J, Farnam Y. Freeze-thaw crack determination in cementitious materials using 3D X-ray computed tomography and acoustic emission. Cem Concr Compos. 2018;89:120-9.
- [36] Shen Y, Wang Y, Wei X, Jia H, Yan R. Investigation on mesodebonding process of the sandstone-concrete interface induced by freeze-thaw cycles using NMR technology. Constr Build Mater. 2020;252:118962.
- Sun M, Zou C, Xin D. Pore structure evolution mechanism of cement mortar containing diatomite subjected to freeze-thaw cycles by multifractal analysis. Cem Concr Compos. 2020;114:103731.
- [38] Guan X, Chen J, Qiu J, Gao Y, Gao J. Damage evaluation method based on ultrasound technique for gangue concrete under freezing-thawing cycles. Constr Build Mater. 2020;246:118437.
- [39] Kong D, Du X, Wei S, Zhang H, Yang Y, Shah SP. Influence of nano-silica agglomeration on microstructure and properties of the hardened cement-based materials. Constr Build Mater. 2012;37:707-15.

- [40] Li D, Niu D, Fu Q, Luo D. Fractal characteristics of pore structure of hybrid Basalt-Polypropylene fibre-reinforced concrete. Cem Concr Compos. 2020;109:103555.
- [41] Fang J, Zhao L, Shi J. Frost resistance and pore structure of concrete incorporated with rubber aggregates and nano-SiO2. Materials. 2021;14:1170.
- [42] Sobolev K, Flores Vivian I, Torres-Martínez L, Cuéllar E, Valdez P, Zarazua E. Performance of cement systems with nano-SiO₂ particles produced using sol-gel method. Mater Res Soc Symp Proc. 2010;1276:10-4.
- [43] GB/T 17671-1999. Method of testing cements-Determination of strength, State Bureau of Building Materials Industry. Chinese National Standard; 1999.
- [44] GB/T 2419-2005. Test method of fluidity of cement mortar. State Bureau of Building Materials Industry. Chinese National Standard; 2005.
- [45] Jiang J, Feng T, Chu H, Wu Y, Wang F, Zhou W, et al. Quasi-static and dynamic mechanical properties of eco-friendly ultra-highperformance concrete containing aeolian sand. Cem Concr Comp. 2019;97:369-78.
- [46] SL/T 352- 2020. Test code for hydraylic concrete, Ministry of Water Resources of the People's Republic of China. Chinese National Standard; 2020.
- [47] Wang J, Guo Z, Yuan Q, Zhang P, Fang H. Effects of ages on the ITZ microstructure of crumb rubber concrete. Constr Build Mater. 2020;254:119329.
- [48] Hu S, Xu Y, Wang J, Zhang P, Guo J. Modification effects of carbon nanotube dispersion on the mechanical properties,

- pore structure, and microstructure of cement mortar. Materials. 2020;13(5):1101.
- [49] Kearsley EP, Wainwright PJ. The effect of porosity on the strength of foamed concrete. Cem Concr Res. 2002;32(2):233-9.
- [50] Li Y, Y, C, He X, Wei J, Guo S. Pore volume fractal dimension of fly ash-cement paste and the relationship between the pore structure and strength. J Chin Ceram Soc. 2003;31:774-9.
- [51] Luping T. A study of the quantitative relationship between strength and pore-size distribution of porous materials. Cem Concr Res. 1986;16(1):87-96.
- [52] Jin NG, Jin XY, Guo JF. Relationship modeling of pore structure and strength of concrete. J Zhejiang Univ. 2005;39(11):1680-4.
- [53] Nili M, Ehsani A. Investigating the effect of the cement paste and transition zone on strength development of concrete containing nanosilica and silica fume. Mater Des. 2015;75:174-83.
- [54] Li W, Shaikh FUA, Wang L, Lu Y, Wang B, Jiang C, et al. Experimental study on shear property and rheological characteristic of superfine cement grouts with nano-SiO2 addition. Constr Build Mater. 2019;228:117046.
- [55] Hou P, Qian J, Cheng X, Shah SP. Effects of the pozzolanic reactivity of nanoSiO2 on cement-based materials. Cem Concr Compos. 2015;55:250-8.
- [56] Kumar R, Bhattacharjee B. Porosity, pore size distribution and in situ strength of concrete. Cem Concr Res. 2003;33(1):155-64.
- [57] Zhuang CL, Chen Y. The effect of nano-SiO₂ on concrete properties: a review. Nanotechnol Rev. 2019;8(1):562-72.